Inorganic Chemistry
Article

Inorg. Chem. **2010**, *49*, 879–887 **879**
DOI: 10.1021/ic901464b

Synthesis and Characterization of Iron(II) Quinaldate Complexes

Dylan T. Houghton, Nicholas W. Gydesen, Navamoney Arulsamy, and Mark P. Mehn*

Department of Chemistry, University of Wyoming, 1000 E. University Avenue, Laramie, Wyoming 82071

Received July 23, 2009

Treatment of iron(II) chloride or iron(II) bromide with 2 equiv of sodium quinaldate (qn=quinaldate or $C_{10}H_6NO_2^-$) yields the coordinatively unsaturated mononuclear iron(II) quinaldate complexes Na[$Fe^{II}(qn)_2Cl$]·DMF and Na-[$Fe^{II}(qn)_2Br$]·DMF (DMF=*N*,*N*-dimethylformamide), respectively. When a similar synthesis is carried out using iron(II) triflate, a solvent-derived linear triiron(II) complex, [$Fe^{II}{}_3(qn)_6(DMF)_2$], with two five-coordinate iron(II) centers and a single six-coordinate iron(II) center is obtained. Each of these species has been characterized using X-ray diffraction. The vibrational features of these complexes are consistent with the observed solid-state structures. Each of these compounds exhibits an iron(II)-to-quinaldate (π^*) charge-transfer band between 520 and 550 nm. These metal-to-ligand charge-transfer bands are sensitive to substitution of the quinaldates as well as alteration of the first coordination sphere ligands. However, the ^{1}H NMR spectra of these paramagnetic high-spin iron(II) complexes are not consistent with retention of the solid-state structures in a DMF solution. The chemical shifts, longitudinal relaxation times (T_1), relative integrations, and substitution of the quinaldate ligands provide a means to fully assign the ^{1}H NMR spectra of the paramagnetic materials. These spectra are consistent with coordination equilibria between five- and six-coordinate species in a DMF solution. Electrochemical studies are reported to place these oxygen-sensitive compounds in a broader context with other iron(II) compounds. Iron complexes of bidentate quinoline-2-carboxylate-derived ligands are germane to metabolic pathways, environmental remediation, and catalytic applications.

Introduction

In the central nervous system, the majority of tryptophan catabolism occurs via the kynurenine pathway.[1] Several of the quinoline- and pyridinecarboxylic acid metabolites formed are important signaling agents in neuronal pathways, which are vital to the onset of certain diseases. For instance, kynurenic acid (4-hydroxyquinoline-2-carboxylic acid) plays a role in glutamate signaling in the brain and is found at elevated levels in people with schizophrenia.[2] Increases in iron concentrations and picolinic acid have been observed in Alzheimer's disease.[3,4] The number of quinoline-2-carboxylic acids found in this pathway and their involvement in brain tumor neuropathology led us to examine the iron(II) coordination chemistry of these metabolites.

Since the initial recognition that quinaldic acid (quinoline-2-carboxylic acid, Hqn) can form complexes with iron(II),[5] the coordination chemistry of quinaldate with iron(II) has received a great deal of attention. Many of the early studies on the determination of binding constants were carried out in water[6−8] and provide the foundation for the use of quinaldic acid in quantitative determinations of the metal content via gravimetric analysis.[9,10] The reaction of an iron(II) salt with either quinaldic acid or sodium quinaldate initially yields a red complex, [$Fe(qn)_2$], which precipitates out of aqueous solution and slowly converts to the dark-blue-violet [$Fe(qn)_2(OH_2)_2$].[11,12] Several structures of iron(II) quinaldate water and alcohol adducts have been reported. The majority of these structures feature a six-coordinate iron(II) geometry with two bidentate quinaldates and two solvent molecules occupying apical positions of a distorted octahedron.[13−18]

*To whom correspondence should be addressed. E-mail: mmehn@uwyo.edu.

(1) Stone, T. W. *Pharmacol. Rev.* **1993**, *45*, 309–379.
(2) Erhardt, S.; Schwieler, L.; Nilsson, L.; Linderholm, K.; Engberg, G. *Physiol. Behav.* **2007**, *92*, 203–209.
(3) Guillemin, G. J.; Cullen, K. M.; Lim, C. K.; Smythe, G. A.; Garner, B.; Kapoor, V.; Takikawa, O.; Brew, B. J. *J. Neurosci.* **2007**, *27*, 12884–12892.
(4) Testa, U.; Louache, F.; Titeux, M.; Thomopoulos, P.; Rochant, H. *Br. J. Hamaetol.* **1985**, *60*, 491–502.
(5) Skraup, H. *Monatsh. Chem.* **1886**, *7*, 210–215.
(6) Wenger, P.-E.; Monnier, D.; Epars, L. *Helv. Chim. Acta* **1952**, *35*, 569–573.
(7) Majumdar, A. K.; Bag, S. P. *Anal. Chim. Acta* **1960**, *22*, 549–553.
(8) Král, M. *Collect. Czech. Chem. Commun.* **1972**, *37*, 46–51.
(9) Vogel, A. I. *Textbook of Quantitative Inorganic Analysis including Elementary Instrumental Analysis*, 4th ed.; Longman: London, 1978.
(10) Kolthoff, I. M.; Sandell, E. B. *Textbook of Quantitative Inorganic Analysis*, 3rd ed.; Macmillan: New York, 1952.
(11) Ray, P.; Bose, M. K. *Z. Anal. Chem.* **1933**, *95*, 400–415.
(12) Bielig, H.-J.; Bayer, E. *Naturwissenschaften* **1953**, *40*, 340.
(13) Okabe, N.; Makino, T. *Acta Crystallogr.* **1998**, *C54*, 1279–1280.
(14) Osawa, K.; Furutachi, H.; Fujinami, S.; Suzuki, M. *Acta Crystallogr.* **2003**, *E59*, m315–m316.
(15) Dobrzyńska, D.; Duczmal, M.; Jerzykiewicz, L. B.; Warchulska, J.; Drabent, K. *Eur. J. Inorg. Chem.* **2004**, 110–117.
(16) Dobrzyńska, D.; Jerzykiewicz, L. B. *J. Chem. Crystallogr.* **2004**, *34*, 51–55.
(17) Dobrzyńska, D.; Jerzykiewicz, L. B.; Duczmal, M. *Polyhedron* **2005**, *24*, 407–412.
(18) Jain, S. L.; Slawin, A. M. Z.; Woollins, J. D.; Bhattacharyya, P. *Eur. J. Inorg. Chem.* **2005**, 721–726.

Published on Web 12/23/2009

There is only one instance of a cis orientation of solvent molecules.[19] Presumably, both cis and trans geometries are accessible in solution.

Despite over a century of experimentation on the coordination chemistry of iron and quinaldate, questions still remain. Reported herein are the syntheses, characterization, and physical properties of a number of iron(II) quinaldate complexes, with the first report of quinaldate supported, anionic, five-coordinate complexes. The single-crystal X-ray diffraction (XRD) patterns have been solved for the coordinatively unsaturated iron(II) complexes **1**, **2**, and **4**. The electronic, IR, and ^{1}H NMR spectra of **1**−**4** are presented. Our ^{1}H NMR results demonstrate that the solid-state structures do not adequately capture the constitution of these compounds in solution. Electrochemical studies of the iron(II) compounds are presented. These studies provide a basis for ongoing work on the reactivity of each of the iron(II) complexes with a variety of oxidants.

Experimental Section

Materials. All manipulations were carried out using standard Schlenk or glovebox techniques under a dinitrogen atmosphere unless otherwise noted. All reagents and solvents were obtained from commercial vendors and used as received unless otherwise noted. Tetrahydrofuran (THF), toluene, benzene, and diethyl ether were distilled under nitrogen from sodium benzophenone and subsequently dried over activated alumina. *N*,*N*-Dimethylformamide (DMF) was stirred over CaH_2 overnight, filtered, vacuum-distilled, and stored under nitrogen. Acetonitrile was distilled from calcium hydride under nitrogen. Nonhalogenated, aprotic solvents were typically tested with a standard purple solution of sodium benzophenone ketyl in THF to confirm effective oxygen and moisture removal. All chemical reactions were performed at high-altitude conditions (~7200 ft or ~2200 m). $Fe(OTf)_2 \cdot 2CH_3CN$ (OTf = $^-OSO_2CF_3$) was prepared according to literature precedent from TMS(OTf) and $FeCl_2$.[20,21] ***Caution!*** *Although we encountered no difficulties, the perchlorate salts of metal complexes with organic ligands are potentially explosive and should be handled with care in small quantities.*

The fluorinated quinaldic acids were prepared under aerobic conditions following modifications of literature precedents.[22,23]

6-Fluoroquinoline-2-aldehyde. To a hot solution of 99% SeO_2 (6.66 g, 60 mmol) in 1,4-dioxane (100 mL) was added 97% 6-fluoro-2-methylquinoline (1.66 g, 10 mmol). The mixture was refluxed for 3 h, filtered while hot, and concentrated by rotary evaporation. The resultant residue was extracted with hot $CHCl_3$ and filtered. The filtrate was washed with two portions of water, followed by a brine wash. The organic layer was dried over $MgSO_4$, and the solvent was removed by rotary evaporation to give the product as a white solid (1.258 g, 72%). ^{1}H NMR ($CDCl_3$, 400 MHz): δ (ppm) 10.21 (s, 1H), 8.27 (m, 2H), 8.06 (d, 1H), 7.60 (m, 1H), 7.53 (m, 1H). ^{13}C ($CDCl_3$, 100 MHz): δ (ppm) 193.5 (s), 162.2 (d, $^1J_{CF}$ = 253 Hz), 152.3 (d, $^4J_{CF}$ = 3 Hz), 145.2 (s), 136.9 (d, $^4J_{CF}$ = 6 Hz), 133.3 (d, $^3J_{CF}$ = 10 Hz), 131.2 (d, $^3J_{CF}$ = 10 Hz), 121.2 (d, $^2J_{CF}$ = 27 Hz), 118.3 (s), 111.2 (d, $^2J_{CF}$ = 22 Hz).

6-Fluoroquinoline-2-carboxylic Acid [H(6-F-qn)]. To a solution of 6-fluoroquinoline-2-aldehyde (0.876 g, 5 mmol) in *tert*-butyl alcohol (100 mL) and 90% 2-methylbut-2-ene (25 mL) was added a solution of 80% sodium chlorite (4.35 g) and 99% sodium dihydrogen phosphate (4.35 g) in water (43.5 mL) over 5 min. The mixture was stirred at room temperature overnight, after which the organic solvents were removed by rotary evaporation. Water was added, and the residue was extracted with CH_2Cl_2, dried over $MgSO_4$, and concentrated by rotary evaporation to give the acid as a white solid (0.8143 g, 85%). ^{1}H ($CDCl_3$, 400 MHz): δ (ppm) 8.39 (d, 1H), 8.31 (d, 1H), 8.20 (m, 1H), 7.64 (m, 1H), 7.58 (m, 1H).

7-Fluoroquinoline-2-aldehyde. To a hot solution of 99% SeO_2 (6.73 g, 60 mmol) in 1,4-dioxane (100 mL) was added 97% 7-fluoro-2-methylquinoline (1.66 g, 10 mmol). The mixture was refluxed for 3 h, filtered while hot, and concentrated by rotary evaporation. The resultant residue was extracted with CH_2Cl_2 and filtered. The filtrate was washed with two portions of water, followed by a brine wash. The organic layer was dried over $MgSO_4$, and the solvent was removed by rotary evaporation to give the product as a white solid (1.375 g, 78%). ^{1}H NMR ($CDCl_3$, 400 MHz): δ (ppm) 10.21(s), 8.32 (d), 8.01 (d), 7.91 (m), 7.88 (m), 7.49 (m). ^{13}C NMR ($CDCl_3$, 100 MHz): δ (ppm) 193.7 (s), 163.7 (d, $^1J_{CF}$ = 252 Hz), 153.5 (s), 149.1 (d, $^3J_{CF}$ = 12 Hz), 137.6 (s), 130.1 (d, $^3J_{CF}$ = 10 Hz), 127.3 (s), 120.0 (d, $^2J_{CF}$ = 26 Hz), 117.0 (s), 114.1 (d, $^2J_{CF}$ = 20 Hz).

7-Fluoroquinoline-2-carboxylic Acid [H(7-F-qn)]. To a solution of 7-fluoroquinoline-2-aldehyde (0.876 g, 5 mmol) in *tert*-butyl alcohol (100 mL) and 90% 2-methylbut-2-ene (25 mL) was added a solution of 80% sodium chlorite (4.35 g) and 99% sodium dihydrogen phosphate (4.35 g) in water (43.5 mL) over 5 min. The mixture was stirred at room temperature overnight, after which the organic solvents were removed by rotary evaporation. Water was added, and the residue was extracted with CH_2Cl_2, dried over $MgSO_4$, and concentrated by rotary evaporation to give the acid as a white solid (0.7834 g, 82%). ^{1}H NMR (D_2O, 400 MHz): δ (ppm) 8.60 (m, 1H). 8.04 (t, 1H), 7.99 (d, 1H), 7.74 (d, 1H), 7.54 (t, 1H).

Na[Fe(qn)$_2$(Cl)]·DMF (1). All of the halide complexes were formed via similar synthetic procedures. Hqn (0.346 g, 2.00 mmol) and NaH (0.0480 g, 2.00 mmol) were added to 10 mL of THF and allowed to stir until gas evolution ceased. $FeCl_2$ (0.127 g, 1.00 mmol) was added to the suspension and the vial rinsed with an additional 5 mL of THF. After stirring overnight, the resultant purple solution was evaporated to dryness in vacuo and the resultant solids were extracted with DMF. The purple solution was filtered and evaporated to dryness. Purple blocks of **1**, suitable for XRD, were grown via vapor diffusion of diethyl ether into a dilute DMF solution over 3 days (yield: 0.362 g, 68.0%). Anal. Calcd for $C_{23}H_{19}ClFeN_3NaO_5$: C, 51.96; H, 3.60; N, 7.90. Found: C, 52.06; H, 3.97; N, 8.24. IR (KBr, cm^{-1}): 1672 [$(CO)_{DMF}$], 1632 [$(COO)_{as}$], 1395 [$(COO)_s$]. ESI/MS (DMF, 200 °C): *m*/*z* 496 ([M − Cl]$^+$, i.e., $Na^+[Fe(qn)_2]\cdot$DMF), 423 ([M − Cl − DMF]$^+$, i.e., $Na^+[Fe(qn)_2]$).

Na[Fe(4-MeO-qn)$_2$(Cl)]·DMF (4-MeO-1). H(4-MeO-qn) (0.2033 g, 1.00 mmol) and NaH (0.0240 g, 1.00 mmol) were added to 5 mL of DMF and allowed to stir until gas evolution ceased. $FeCl_2$ (0.0638 g, 0.50 mmol) was added to the suspension and the vial rinsed with an additional 5 mL of DMF. After stirring overnight, the resultant dark red/purple solution was filtered and evaporated to dryness. The solid was dissolved in DMF and filtered, and dark-red crystals of **4-MeO-1** were obtained by vapor diffusion of diethyl ether into the solution (yield: 0.249 g, 84.3%). IR (KBr, cm^{-1}): 1653 [$(COO)_{as}$], 1390 [$(COO)_s$]. ESI/MS (DMF, 200 °C): *m*/*z* 556 ([M − Cl]$^+$, i.e., $Na^+[Fe(4\text{-MeO-qn})_2]\cdot$DMF), 483 ([M − Cl − DMF]$^+$, i.e., $Na^+[Fe(4\text{-MeO-qn})_2]$).

Na[Fe(6-F-qn)$_2$(Cl)]·DMF (6-F-1). H(6-F-qn) (0.1914 g, 1.00 mmol) and NaH (0.0240 g, 1.00 mmol) were added to 5 mL of DMF and allowed to stir until gas evolution ceased. $FeCl_2$ (0.0636 g, 0.50 mmol) was added to the suspension and the vial rinsed with an additional 5 mL of DMF. After stirring overnight, the resultant purple solution was filtered and evaporated

(19) Okabe, N.; Muranishi, Y. *Acta Crystallogr.* **2003**, *E59*, m220–m222.
(20) Hagadorn, J. R.; Que, L., Jr.; Tolman, W. B. *Inorg. Chem.* **2000**, *39*, 6086–6090.
(21) Hagen, K. S. *Inorg. Chem.* **2000**, *39*, 5867–5869.
(22) Bu, X.; Deady, L. W.; Finlay, G. J.; Baguley, B. C.; Denny, W. A. *J. Med. Chem.* **2001**, *44*, 2004–2014.
(23) Contour-Galcéra, M.-O.; Sidbu, A.; Plas, P.; Roubert, P. *Bioorg. Med. Chem. Lett.* **2005**, *15*, 3555–3559.

to dryness. The solid was dissolved in DMF and filtered, and purple crystals of **6-F-1** were obtained by vapor diffusion of diethyl ether into the solution (yield: 0.258 g, 91.0%). IR (KBr, cm^{-1}): 1650 [br, $(COO)_{as}$], 1358 [$(COO)_s$]. ESI/MS (DMF, 200 °C): m/z 532 ($[M - Cl]^+$, i.e., $Na^+[Fe(6\text{-}F\text{-}qn)_2]\cdot DMF$), 517 ($[M - Cl - DMF]^+$, i.e., $Na^+[Fe(6\text{-}F\text{-}qn)_2]$).

Na[Fe(6-F-qn)$_2$(Cl)]·DMF (7-F-1). H(6-F-qn) (0.1912 g, 1.00 mmol) and NaH (0.0240 g, 1.00 mmol) were added to 5 mL of DMF and allowed to stir until gas evolution ceased. $FeCl_2$ (0.0637 g, 0.50 mmol) was added to the suspension and the vial rinsed with an additional 5 mL of DMF. After stirring overnight, the resultant purple solution was filtered and evaporated to dryness. The solid was dissolved in DMF and filtered, and purple crystals of **7-F-1** were obtained by vapor diffusion of diethyl ether into the solution (yield: 0.262 g, 92.3%). IR (KBr, cm^{-1}): 1650 [br, $(COO)_{as}$], 1360 [$(COO)_s$]. ESI/MS (DMF, 200 °C): m/z 532 ($[M - Cl]^+$, i.e., $Na^+[Fe(7\text{-}F\text{-}qn)_2]\cdot DMF$), 517 ($[M - Cl - DMF]^+$, i.e., $Na^+[Fe(7\text{-}F\text{-}qn)_2]$).

Na[Fe(qn)$_2$(Br)]·DMF (2). 2 was prepared in a manner similar to that of **1** using $FeBr_2$ (0.216 g, 1.00 mmol). Purple blocks of **2**, suitable for XRD, were grown via vapor diffusion of diethyl ether into a dilute DMF solution over 3 days (yield: 0.501 g, 87%). Anal. Calcd for $C_{23}H_{19}BrFeN_3NaO_5$: C, 47.95; H, 3.32; N, 7.29. Found: C, 47.91; H, 3.19; N, 7.34. IR (KBr, cm^{-1}): 1677 $[(CO)_{DMF}]$, 1632 $[(COO)_{as}]$, 1393 $[(COO)_s]$. ESI/MS (DMF, 200 °C): m/z 496 ($[M - Br]^+$, i.e., $Na^+[Fe(qn)_2]\cdot DMF$), 423 ($[M - Br - DMF]^+$, i.e., $Na^+[Fe(qn)_2]$).

Fe(qn)$_2$(DMF) (3). 3 was prepared in a manner similar to that of **1** using FeI_2 (0.3097 g, 1.00 mmol). A powder of **3** was obtained via vapor diffusion of diethyl ether into a saturated DMF solution over 3 days (yield: 0.3607 g, 76.2%). Anal. Calcd for $C_{23}H_{19}FeN_3O_5$: C, 58.37; H, 4.05; N, 8.88. Found: C, 58.56; H, 4.57; N, 8.80. IR (KBr, cm^{-1}): 1657 $[(CO)_{DMF}]$, 1612 $[(COO)_{as}]$, 1384 $[(COO)_s]$. ESI/MS (DMF, 200 °C): m/z 496 ($[M + Na]^+$, i.e., $Na^+[Fe(qn)_2]\cdot DMF$), 423 ($[M - DMF + Na]^+$, i.e., $Na^+[Fe(qn)_2]$).

[Fe$_3$(qn)$_6$(DMF)$_2$]·4DMF (4). Hqn (0.346 g, 2.00 mmol) and NaH (0.0480 g, 2.00 mmol) were dissolved in 10 mL of THF and allowed to stir for 2 min (before they were fully dissolved). $Fe(OTf)_2\cdot 2CH_3CN$ (0.412 g, 1.00 mmol) was added to the solution and the vial rinsed with an additional 5 mL of THF. After stirring overnight, the resultant deep-red solution was filtered and evaporated to dryness in vacuo, yielding a deep-red powder. IR (KBr, cm^{-1}): 1669 $[(COO)_{as}]$, 1383 $[(COO)_s]$. Purple blocks of **4**, suitable for XRD, were grown via vapor diffusion of diethyl ether into a saturated DMF solution of **4** over 5 days (yield: 0.3720 g, 68.1%). Anal. Calcd for $C_{78}H_{78}Fe_3N_{12}O_{18}$: C, 57.16; H, 4.80; N, 10.25. Found: C, 57.51; H, 4.86; N, 10.01. IR (KBr, cm^{-1}): 1657 $[(COO)_{DMF}]$, 1612 $[(COO)_{as}]$, 1338 $[(COO)_s]$. ESI/MS (DMF, 200 °C): m/z 496 ($[M + Na]^+$, i.e., $Na^+[Fe(qn)_2]\cdot DMF$), 423 ($[M - DMF + Na]^+$, i.e., $Na^+[Fe(qn)_2]$).

***trans*-[Fe(qn)$_2$(PrOH)$_2$].** This compound was prepared according to literature precedent.[15]

Physical Methods. Elemental analyses were performed at Columbia Analytical Services Inc., Tuscon, AZ. ^1H and ^{13}C NMR were collected on a Bruker Avance DRX-400 NMR spectrometer at room temperature unless otherwise noted. For paramagnetic samples, special care was taken to ensure that the delay between pulses was greater than 5 times the longest proton longitudinal relaxation time (T_1) for proper integration of peaks. UV−vis spectra were recorded on an Agilent 8453 diode-array spectrophotometer at room temperature. A Varian 800 FT-IR spectrometer with a resolution of 1 cm^{-1} was used to record IR spectra of the KBr pellets of the samples. Electrochemical measurements were carried out in a drybox under dinitrogen in a DMF solution with 0.1 M $(^nBu_4N)(ClO_4)$ as the supporting electrolyte using a model CS-1200 computer-controlled potentiostat (Cypress Systems). A three-electrode configuration with a glassy carbon working electrode, a Ag/$AgNO_3$ (0.1 M in CH_3CN) reference electrode, and a platinum wire auxiliary electrode was used. The potential values were referenced to an internal ferrocenium/ferrocene couple, which is reported to be +0.47 V vs SCE in 0.1 M $(^nBu_4N)(ClO_4)$ in DMF.[24] The peak separations are reported with a scan rate of 200 mV/s (the $Fc^{+/0}$ peak separation was 90 mV under these conditions). The electrospray ionization mass spectral (ESI/MS) data for the compounds were obtained using an LCQ mass spectrometer (Finnigan MAT) on DMF solutions that were directly infused into the spectrometer via a syringe pump. The heated capillary was set at 200 °C.

Table 1. Summary of Crystallographic Data for **1**, **2**, and **4**

	1	**2**	**4**
chemical formula	$C_{23}H_{19}Cl$-FeN_3NaO_5	$C_{23}H_{19}Br$-FeN_3NaO_5	$C_{78}H_{78}$-$Fe_3N_{12}O_{18}$
fw (g/mol)	531.70	576.16	1639.07
space group	$P2(1)/n$	$P2(1)/n$	$P\bar{1}$
a (Å)	9.9545(2)	9.9868(2)	10.4573(2)
b (Å)	15.2180(3)	15.3065(3)	13.2512(3)
c (Å)	15.1842(3)	15.3134(3)	14.1832(3)
α (deg)	90	90	85.557(1)
β (deg)	94.6620(10)	94.076(1)	87.301(1)
γ (deg)	90	90	73.295(1)
V (Å^3)	2292.61(8)	2334.93(8)	1876.16(7)
Z	4	4	1
D_{calcd} (mg/m^3)	1.540	1.639	1.451
temp (K)	100(2)	150(2)	150(2)
abs coeff (mm^{-1})	0.834	2.146	0.652
R1 [$I > 2\sigma(I)$][a]	0.0481	0.0431	0.0378
wR2 [$I > 2\sigma(I)$][b]	0.1127	0.1068	0.0948

[a] $R1 = \sum||F_o| - |F_c||/\sum|F_o|$. [b] $wR2 = [\sum w(F_o^2 - F_c^2)^2]/\sum w(F_o^2)^2]]^{1/2}$ where $w = q/\sigma^2(F_o^2) + (a^*P)^2 + b^*P$.

XRD Analysis. 1, **2**, and **4** were characterized using XRD. A purple diamond-shaped crystal of **1**, a purple rectangular plate of **2**, and a purple rectangular plate of **4** were glued to a MiTeGen micromount using Paratone N oil and mounted on a Bruker Smart Apex II CCD area detector for data collection at either 100 or 150 K using graphite-monochromated Mo Kα ($\lambda = 0.710\,73$ Å) radiation. A summary of the crystallographic details is given in Table 1. All non-hydrogen atoms were refined anisotropically, whereas the hydrogen atoms were placed in ideal positions and refined as riding atoms with relative isotropic displacement parameters. The final full-matrix least-squares refinement converged to R1 = 0.0481 and wR2 = 0.1290 for **1**, R1 = 0.0431 and wR2 = 0.1224 for **2**, and R1 = 0.0378 and wR2 = 0.1134 for **4**.

Results and Discussion

Mononuclear iron(II) quinaldate complexes were anaerobically synthesized by the addition of 2 equiv of sodium quinaldate to a variety of simple iron salts in THF (Scheme 1). Single crystals suitable for XRD analysis were grown via the slow diffusion of diethyl ether into DMF solutions of **1** and **2**. We have only obtained needles of **3**, which proved unsuitable for XRD analysis from the iron(II) iodide synthesis. Interestingly, when similar reaction conditions are employed with $[Fe(OTf)_2]\cdot 2CH_3CN$, a deep-red powder is obtained, which we believe to be analogous to the previously reported $[Fe(qn)_2]$.[12,17] Although the elemental analysis is convincing,[12] the ambiguous magnetic properties and absence of XRD data of the proposed complex did not provide conclusive evidence for this formulation.[17] Unlike the previously reported red-black species, our complex is not

(24) Connelly, N. G.; Geiger, W. E. *Chem. Rev.* **1996**, *96*, 877–910.

Scheme 1

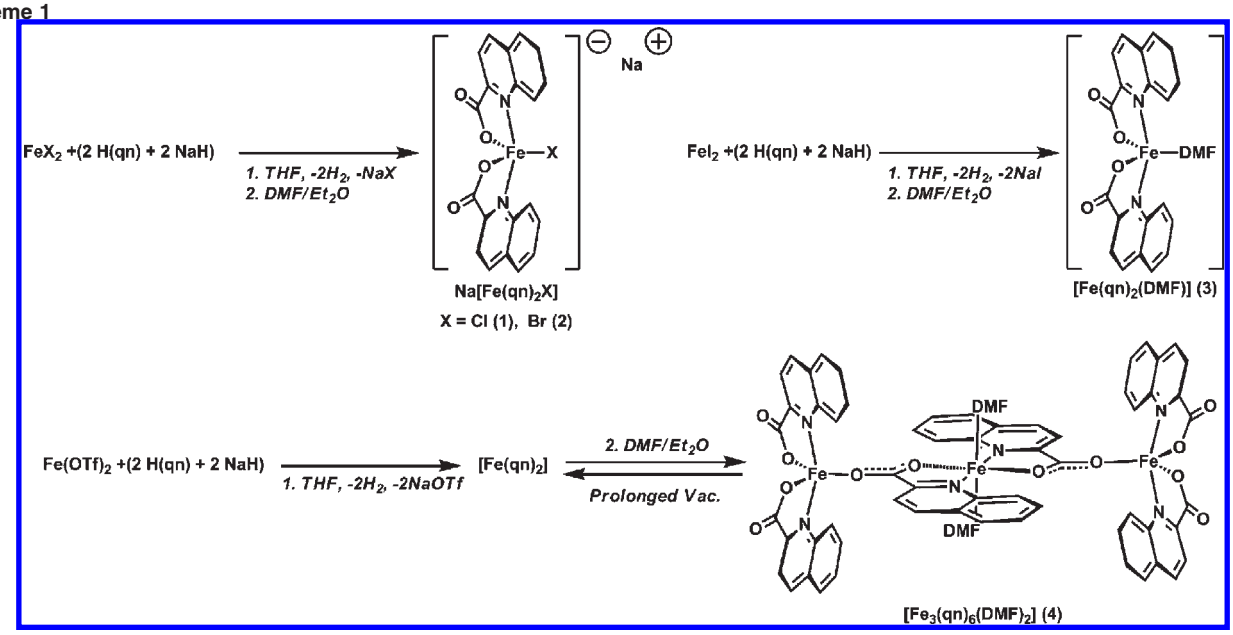

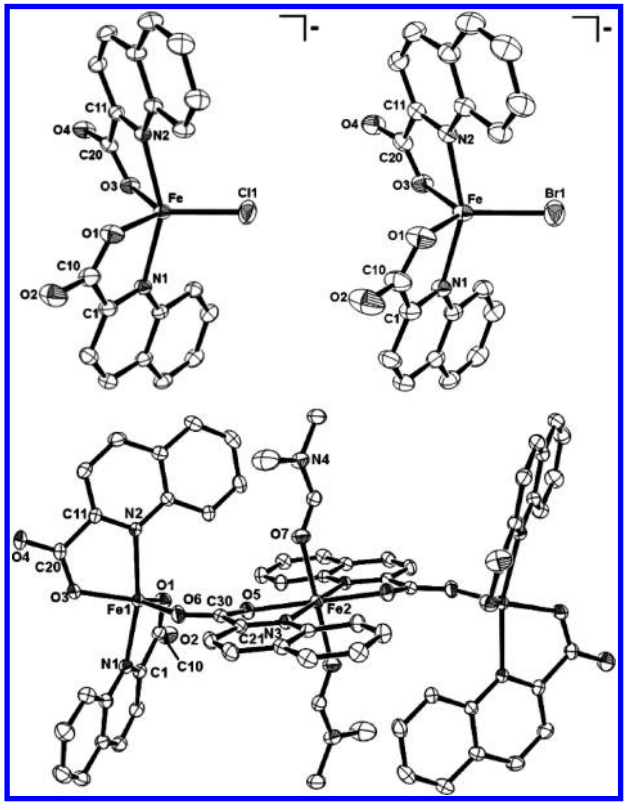

Figure 1. ORTEP plot of the anions of **1** and **2** (top) and the triiron complex **4** (bottom) showing 50% probability thermal ellipsoids and the labeling scheme for selected atoms. Only half of the symmetric trimer has been labeled. Hydrogen atoms, cocrystallized DMF, and the sodium cation from **1** and **2** are omitted for clarity.

soluble in chloroform or dichloromethane.[12,17] When dissolved in DMF, a color change to dark purple is immediately observed. Prolonged exposure of the purple solution to vacuum yields a dark-red powder consistent with a reversible equilibrium. Diffusion of diethyl ether into a saturated DMF solution yields purple crystals of the triiron complex **4**.

Table 2. Selected Bond Lengths (Å) and Angles (deg) for **1**, **2**, and **4**

			4	
	1	**2**	5C−Fe1	6C−Fe2[a]
Fe−O1	2.0413(11)	2.030(2)	2.0079(11)	2.1541(11)
Fe−O3	2.0705(11)	2.061(2)	2.0166(11)	
Fe−N1	2.1895(14)	2.197(2)	2.1704(13)	2.2550(12)
Fe−N2	2.1890(13)	2.198(2)	2.1803(12)	
Fe−X	2.2788(5)	2.4309(5)	2.0459(12)	2.0738(11)
O1−Fe−X	125.08(4)	124.86(7)	119.57(5)	92.78(5), 87.22(5)
O1−Fe−N1	77.67(5)	77.74(8)	78.84(5)	74.90(4)
O3−Fe−N2	76.60(4)	76.94(7)	78.18(5)	
O1−Fe−N2	86.60(5)	87.22(8)	97.74(5)	105.10(4)
O1−Fe−O3	115.04(5)	115.61(9)	128.96(5)	180.00(5)
O3−Fe−X	119.77(4)	119.45(6)	111.40(5)	92.78(5)
O3−Fe−N1	89.92(5)	90.77(8)	92.32(5)	105.10(4)
N1−Fe−N2	152.70(5)	154.27(8)	164.74(5)	180.0
N1−Fe−X	104.86(4)	103.86(6)	97.90(5)	96.06(4), 83.94(4)
N2−Fe−X	102.43(4)	101.86(6)	96.70(5)	
τ^{25}	0.55	0.58	0.60	

[a] Comparable distances are compared although the numbering of the individual sites differs.

Structures of Iron(II) Quinaldates. All of the previously crystallographically characterized iron(II) quinaldate compounds contain coordinatively saturated iron centers and are neutral complexes. The crystal structure of **1** reveals a five-coordinate iron(II) center with two quinaldate chelates and a single chloride, to yield the complex anion (Figure 1, top left, and Table 2). The iron(II) center is best described as a distorted trigonal bipyramid (τ = 0.55).[25] The principal axis through the iron(II) center is defined by the nitrogen atoms of the two quinaldates [N1−Fe−N2 = 152.70(5)°], while the more tightly bound carboxylates and the chloride define the trigonal plane.

(25) Addison, A. W.; Rao, T. N.; Reedijk, J.; van Rijn, J.; Verschoor, G. C. *J. Chem. Soc., Dalton Trans.* **1984**, 1349–1356.

Table 3. Summary of Physical Properties and Comparisons with Literature Precedents

	color	ν_{sym}(COO) (cm^{-1})	ν_{asym}(COO) (cm^{-1})	ν_{DMF}(C=O) (cm^{-1})	λ (nm) [ε (M^{-1} cm^{-1})]		E (mV) vs $Fc^{+/0}$	ref
1	purple	1395	1632	1672	546 [730]	381 [307]	−334 (113)	a
4-MeO-1	dark red	1390	1653 (br)		530 [596]	370 [592]; 345 [882]	−393 (96)	a
6-F-1	purple	1358	1650 (br)		549 [590]	371 [309]	−288 (84)	a
7-F-1	purple	1360	1650 (br)		550 [592]	368 [314]	−300 (75)	a
2	purple	1393	1632	1677	534 [980]	375 [384]	−216 (99)	a
3	purple	1384	1612	1657	527 [775]	368 [274]	−167 (75)	a
precursor to **4**	dark red	1383	1669					a
$[Fe(qn)_2]$	red-black	1377	1652		556			17
4	purple	1338	1612	1657	530 [1180]	376 [373]	−170 (88)	a
Na(qn)		1393	1647					17
trans-$[Fe(qn)_2(pyr)_2]$	purple	1361	1652					18
trans-$[Fe(qn)_2(H_2O)_2]$	deep red	1399	1619		539			17
trans-$[Fe(qn)_2(MeOH)_2]$	brown	1387	1635					18
trans-$[Fe(qn)_2(EtOH)_2]$	red-violet		1628		527 [800]			14
trans-$[Fe(qn)_2(PrOH)_2]$	purple	1394	1628		528 [1010][a]	371 [326][a]	−160 (83)[a]	

[a] This work.

The iron−carboxylate distances are consistent with those observed in other high-spin iron(II) complexes.[20,26,27] A comparison of geometric parameters in all known iron(II) quinaldates is provided in the Supporting Information (Table S1). The presence of a sodium cation confirms the binding of the quinaldates in the deprotonated state. The crystal structure of quinaldic acid exhibits a greater disparity between the carboxylate bond distances [1.314(2) and 1.221(2) Å],[16] which further supports the deprotonation of the carboxylate in this compound. The five-membered chelate rings of the iron quinaldate complexes are nearly planar, exhibiting no torsion angles over 11°. The structure of the bromide **2** is similar to that of the chloride (Figure 1, top right). The longer iron−bromide distance is accompanied by a shortening of the Fe−O bonds in the trigonal plane.

Analysis of the dark-purple crystals of **4** reveals a symmetric triiron complex containing both five- and six-coordinate iron(II) centers (Figure 1, bottom, and Table 2). Two quinaldate chelates support each iron center; however, the carboxylates from the central iron center also contribute to the coordination sphere of the terminal five-coordinate iron centers. The geometry of these capping iron centers is best described as a distorted trigonal bipyramid ($\tau = 0.60$). As in the chloride complex **1**, the principal axis of the trigonal bipyramid is defined by the two nitrogen donors [N1−Fe−N2 = 164.74(5)°], while the carboxylate oxygen atoms reside in the trigonal plane. The slightly distorted octahedral geometry of the central iron center contains two quinaldate chelate rings in the equatorial plane. Two DMF molecules complete the coordination sphere of the central iron. Although the chelate angles do not change significantly (N3−Fe−O5 = 77°), the bond distances of the iron ligands appreciably lengthen when changing from five- to six-coordinate iron(II) centers. Furthermore, the change in the C−O bond distances supports a fully delocalized carboxylate for the central quinaldates (Table S1 in the Supporting Information).

Properties of Iron(II) Complexes. The IR spectra of the iron(II) quinaldate complexes were collected as KBr pellets (Table 3 and Figure S1 in the Supporting Information). In **1**, three strong features at 1672, 1632, and 1395 cm^{-1} can be identified. On the basis of the observed spectra and literature precedents,[14,15,18,28,29] we tentatively assign the band at 1672 cm^{-1} to cocrystallized DMF retained in the KBr pellets, and the features at 1395 and 1632 cm^{-1} to symmetric and asymmetric carboxylate stretches. As shown in Table 3, the separation between the symmetric and asymmetric bands ranges from 220 to 291 cm^{-1}. These values are consistent with the carboxylate coordination modes observed in the solid state.[28] Attempts to attain vibrational information for the complexes in solution have been unsuccessful because of intense DMF solvent features. The complexes are insoluble in other solvents.

The iron(II) quinaldate complexes undergo no noticeable change in color upon dissolution of the crystals in DMF. $[Fe(qn)_2(Cl)]^-$ exhibits an intense feature at 546 nm (18 300 cm^{-1}) with a less intense band at 381 nm (26 250 cm^{-1}; Figure 2A and Table 3). Upon a change in the fifth ligand to bromide (Figure 2B), a shift to higher energy is observed for each feature, namely, 534 nm (18 730 cm^{-1}) and 375 nm (26 670 cm^{-1}). Furthermore, the substituted quinoline complexes provide additional evidence for an iron(II)-to-quinaldate charge-transfer assignment. While 6-F-qn and 7-F-qn substitutions perturb the spectrum relatively little, $[Fe(4\text{-MeO-qn})_2(Cl)]^-$ exhibits a distinct electronic spectrum (Figure S2 in the Supporting Information). A clear change in the position of the charge-transfer band to 530 nm (18 900 cm^{-1}), as well as two high-energy features at 370 nm (27 030 cm^{-1}) and 342 nm (29 240 cm^{-1}), is observed. When the additional ligand(s) are solvent molecules, a further shift to higher energy is seen. **3**, **4**, and *trans*-$[Fe(qn)_2(PrOH)_2]$ all exhibit bands at ∼530 nm (18 870 cm^{-1}) and ∼372 nm (26 881 cm^{-1}) in DMF.

(26) Friese, S. J.; Kucera, B. E.; Young, V. G., Jr.; Que, L., Jr.; Tolman, W. B. *Inorg. Chem.* **2008**, *47*, 1324–1331.
(27) LeCloux, D. D.; Barrios, A. M.; Mizoguchi, T. J.; Lippard, S. J. *J. Am. Chem. Soc.* **1998**, *120*, 9001–9014.
(28) Deacon, G. B.; Phillips, R. J. *Coord. Chem. Rev.* **1980**, *33*, 227–250.
(29) Nakamoto, K. *Infrared and Raman Spectra of Inorganic and Coordination Compounds Part B: Applications in Coordination, Organometallic and Bioinorganic Chemistry*, 5th ed.; John Wiley & Sons, Inc.: New York, 1997.

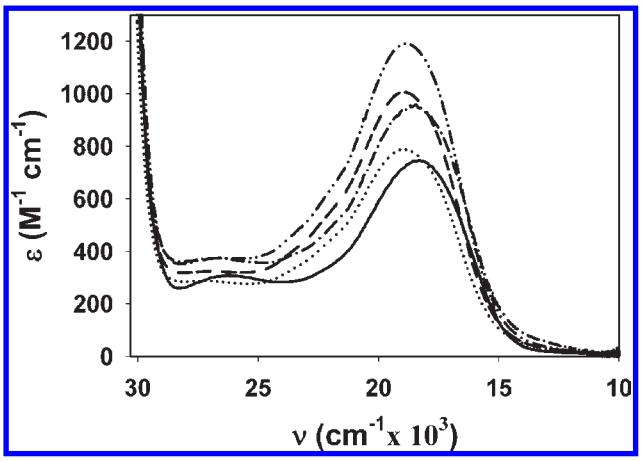

Figure 2. Electronic spectra of iron(II) quinaldate complexes recorded at room temperature in DMF: (A) **1** (—); (B) **2** (−·−); (C) **3** (···); (D) **4** (−···−); (E) *trans*-[Fe(qn)$_2$(PrOH)$_2$] (− −).

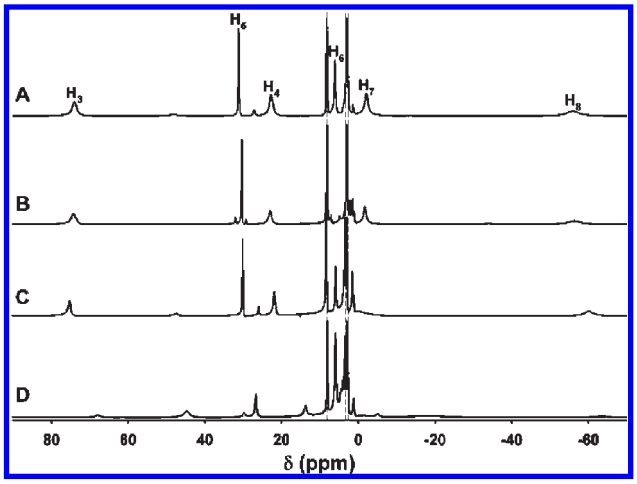

Figure 3. ^{1}H NMR spectrum of (A) **1**, B) **6-F-1**, (C) **7-F-1**, and (D) **4-MeO-1** in DMF-d_7 at room temperature. Spectra are referenced to the residual protic solvent peak at 8.03 ppm. Dashed lines identify the peaks associated with DMF resonances.

The high extinction coefficients and observed shifts are consistent with literature precedent of assigning these features to metal-to-ligand charge-transfer bands.[14,17] Kral reported three bands in the electronic spectrum of *trans*-[Fe(qn)$_2$(H$_2$O)$_2$] in an aqueous acetate buffer at 440 nm (500 M^{-1} cm^{-1}, $\pi \rightarrow e_g$), 513 nm (500 M^{-1} cm^{-1}, $t_{2g} \rightarrow \pi^*$), and 800 nm (19 M^{-1} cm^{-1}, $^5T_{2g} \rightarrow {}^5E_g$).[8,30] Guided by Kral's assignments, we would expect a ligand-field band at 670 nm, which we do not observe. Even when a 10 cm cell is utilized, no d−d transitions are detected in the near-IR for any of these iron(II) quinaldate complexes (out to 1100 nm or ∼9100 cm^{-1}). A very weak shoulder is observed at low energy for *trans*-[Fe(qn)$_2$(PrOH)$_2$] in DMF.

The ^{1}H NMR spectra of the paramagnetic high-spin iron(II) complexes have been analyzed in DMF-d_7 (Figures 3 and 4 and Table 4). Assignments have been made on the basis of chemical shifts, longitudinal relaxation measurements (T_1), relative integration,

(30) Independent synthesis of the iron acetate complex results in a dark-blue solution, which by NMR and CV is a mixture of multiple species. The presence of acetate may confound Kral's assignments.

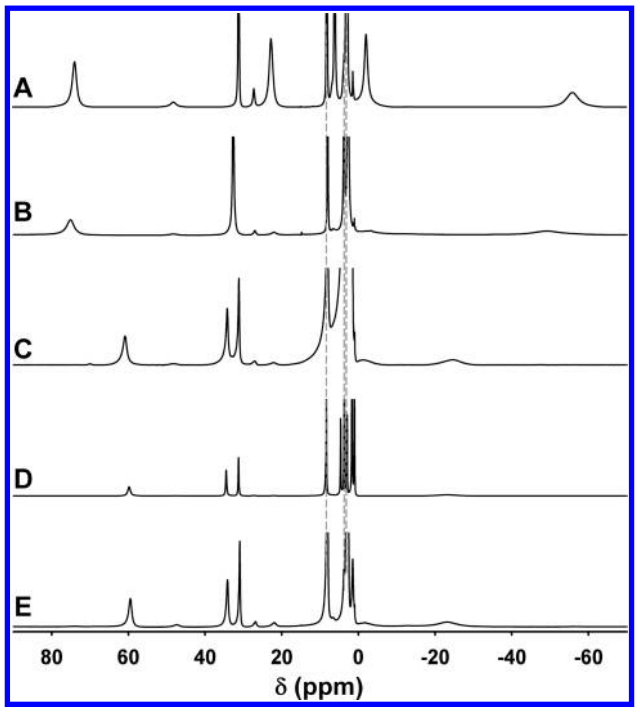

Figure 4. ^{1}H NMR spectrum of (A) **1**, B) **2**, (C) **3**, (D) *trans*-[Fe(qn)$_2$-(PrOH)$_2$], and (E) **4** in DMF-d_7 at room temperature. Spectra are referenced to the residual protic solvent peak at 8.03 ppm. Dashed lines identify the peaks associated with DMF resonances.

substitution, and variable-temperature studies. A rapid inspection of the room temperature ^{1}H NMR spectrum of freshly dissolved crystals of **1** reveals at least 12 peaks (Figure 3A), several more than expected considering that the quinaldate ligands are in a symmetric environment. Furthermore, the resonances can be grouped into two groups of six with notable differences in their relative intensities (1.00:0.16). This is consistent with a major species being in equilibrium with another minor species. The addition of [Me$_3$PhN]Cl to samples of **1** does not affect the relative intensities of these peaks. Increasing the temperature results in changes in the chemical shifts of the peaks and the relaxation times (i.e., the breadth of the peaks) as well as a coalescence of the resonances observed for the two species (Figures S3−S6 in the Supporting Information). Therefore, we believe the best candidate is an equilibrium between a five-coordinate species and a six-coordinate [Fe(qn)$_2$(Cl)(DMF)] species.

$$[Fe(qn)_2(Cl)]^- + DMF \leftrightarrow [Fe(qn)_2(Cl)(DMF)]^- \quad (1)$$

The assignments for the six major peaks in **1** will be discussed as an example of the process used for the other complexes. In the spectrum of **1**, the very broad peak observed at −58 ppm with the very fast relaxation time (0.8 ms) is assigned to the H$_8$ position. This is consistent with the average Fe---H$_n$ distances taken from the reported crystallographic data showing H$_8$ being in closest proximity to the iron(II) center both through space and through bond (Scheme 2). The peak with the largest downfield shift (71 ppm) has an integration of one proton and a short T_1 of 3.8 ms. It has been assigned to the 3 position of the quinaldate ring, which is also quite near the metal center (Scheme 2). The substituted complexes

Table 4. Summary of ^{1}H NMR Parameters[a]

	H_3-qn δ (ppm)	H_4-qn δ (ppm)	H_5-qn δ (ppm)	H_6-qn δ (ppm)	H_7-qn δ (ppm)	H_8-qn δ (ppm)
1	71 (3.8)	21 (14)	32(24)	6 (28)	−2 (8.3)	−58 (0.3)
4-MeO-1	69	4[OMe]	30	14	−5	−64
6-F-1	74	23	30	--	−2	−56
7-F-1	75	22	30	6	--	−60
2	75 (3.2)	33 (12)	33 (12)	4 (21)	−2	−49 (0.2)
3	61(2)	34 (12)	31 (19)	4	0	−25 (0.2)
trans-[Fe(qn)$_2$(PrOH)$_2$]	60 (2.9)	34 (8.9)	31 (15)	4	2	−23 (0.2)
4	59 (2.4)	34 (8.7)	31 (15)	4 (15)	1 (19)	−23 (0.1)

[a] All spectra are recorded in DMF-d_7. Numbers in parentheses are relaxation times (T_1) in milliseconds.

Scheme 2. Numbering and Average XRD Fe---H_n Distances

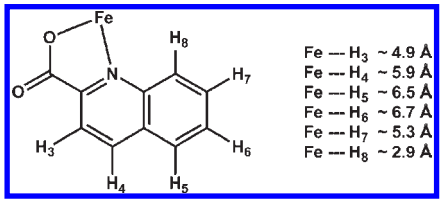

allow us to watch for systematic absences in the ^{1}H NMR spectra and to unambiguously assign the remaining resonances. The spectrum of **6-F-1** displays no resonance at 6 ppm (Figure 3B); therefore, we assign this peak to H_6. Similarly, **7-F-1** exhibits no peak at −2 ppm (Figure 3C). This leads us to assign the H_7 resonance to the peak at −2 ppm, consistent with its shorter T_1 value. **4-MeO-1** eliminates the H_4 resonance at 21 ppm in **1** with the appearance of a new methyl group resonance (integrating for three protons) at 4 ppm (Figure 3D). Therefore, the best candidate for the H_4 resonance in **1** is the peak at 21 ppm (T_1 = 14 ms). This substitution also shifts the H_6 proton resonance from 6 to 14 ppm (integrating for one proton). The single remaining resonance of sufficient integration is the peak at 32 ppm, which we assign to H_5. The longer T_1 value of H_5 relative to H_4 is also consistent with the increased through-space distance to the iron center. It is noteworthy that neither an σ-spin nor a π-spin delocalization pathway appears to dominate in this aromatic quinoline ring system. The short relaxation times of each of these resonances give insufficient time for spin mixing before equilibrium is restored precluding the observation of COSY cross-peaks.

With the major peaks assigned, the assignment of the minor resonances should be addressed. On the basis of the substituted complexes (Figure 3), we can confidently ascribe the peaks to two sets of quinaldate rings from two complexes in which the respective ligands are in magnetically inequivalent environments. The 4-MeO-qn complex shows an inversion in the intensities of the peaks corresponding to the major and minor species (eq 1). The electron-donating substituent presumably gives rise to a less Lewis acidic metal center.[31] Therefore, we believe the five-coordinate geometry is the major species in [Fe(4-MeO-qn)$_2$Cl]$^-$ (Figure 3D), while the six-coordinate [Fe(qn)$_2$(Cl)(DMF)] is the major species in solutions of **1** (Figure 3A). This is not the sole possibility for the observed equilibria. For instance, a cis/trans isomerization, a different coordination equilibrium, or a ligand rearrangement may also result in two sets of quinaldate signals. The relative integrations of the major and minor peaks do not support two inequivalent quinaldates bound to the same metal center. The concentration of the analyte does not noticeably affect the ratio of the peaks, so we do not favor the formation of a coordination polymer (similar to **4**) in a DMF solution.

The ^{1}H NMR spectrum of **2** (Figure 4B) was assigned based on its similarity to that of **1**. One notable exception is the peak at 33 ppm, which integrates for two protons. The variable-temperature ^{1}H NMR spectra give rise to two separate peaks of different widths for the H_4 and H_5 resonances, providing further support for the assignment of these spectral features (Figure S5 in the Supporting Information). On the basis of its similarity to **1** and the variable-temperature experiments, we assign the feature at 33 ppm in the room temperature spectrum to the H_4 and H_5 protons. Notably, the H_6 resonance is shifted to 4 ppm and broadened in **2**, making it harder to distinguish from the solvent peak; however, a T_1 of 21 ms was measured, akin to that observed in **1**. Also, the H_7 resonance is greatly broadened in **2**, prohibiting a T_1 measurement of this peak.

The ^{1}H NMR spectra of **3**, *trans*-[Fe(qn)$_2$(PrOH)$_2$], and the triiron complex **4** are essentially indistinguishable (Figure 4C−E and Table 4). The spectrum of the complex formed upon dissolving **3** in DMF exhibits four paramagnetically shifted peaks for the quinaldate ligands, with the remaining two very broad peaks at 4 and 2 ppm (Figure 4C). These assignments are summarized in Table 4.[32] Interestingly, a similar set of peaks is observed after dissolving the coordination polymer **4** in DMF. *trans*-[Fe(qn)$_2$(PrOH)$_2$] exhibits the same paramagnetically shifted peaks. Additionally, peaks for propanol are observed in the diamagnetic region without paramagnetic broadening. This is consistent with DMF displacing the propanol ligands in solution. The similarity in the NMR responses leads us to propose that the same moiety is being formed in each solution. Furthermore, when DMF solutions of **3**, **4**, and/or *trans*-[Fe(qn)$_2$(PrOH)$_2$] are mixed, no spectral changes are observed in the ^{1}H NMR spectra.

On the basis of literature precedent and the coordination of the central iron center in the trimer, [Fe(qn)$_2$-(DMF)$_2$] is a likely candidate for the species formed in

(31) Xue, G.; Fiedler, A. T.; Martinho, M.; Münck, E.; Que, L., Jr. *Proc. Natl. Acad. Sci. U.S.A.* **2008**, *105*, 20615–20620.

(32) Although Jain and co-workers[18] did report NMR spectra for [Fe(qn)$_2$(MeOH)$_2$] in DMF-d_7, we believe that the quickly relaxing peaks (60 and −23 ppm) were inadvertently omitted from their spectra. We do not observe peaks at 12, 4.4, or 2.3 ppm. Furthermore, our independent synthesis of the methanol adduct returns a purple complex, which turns brown upon oxidation.

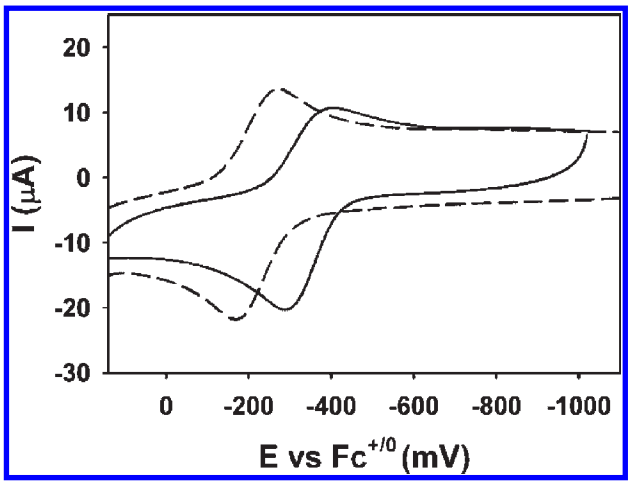

Figure 5. Cyclic voltammograms of 1 mM **1** (—) and **2** (− −) in DMF with 0.1 M (^{n}Bu$_4$N)(ClO$_4$) as the supporting electrolyte at a scan rate of 200 mV/s.

solution. DMF solutions of the solvent adducts also give identical positive-ion ESI patterns with notable peaks at m/z 496 (i.e., $Na^+[Fe(qn)_2]\cdot DMF$) and 423 (i.e., $Na^+[Fe(qn)_2]$). Despite our best efforts, we see no evidence for $[Fe(qn)_2(DMF)_2]$ in the gas phase. These results only provide constitution of the ions observed and yield no information on the connectivity of the nuclei in the gas phase.

The ^{1}H NMR of the solvent adducts also exhibit a second set of quinaldate peaks with significantly lower integration (Figure 4C,D). The intensity of these peaks is insensitive to the precursor (i.e, **3**, **4**, or propanol adduct) used to generate the sample as well as to the concentration of the complex in DMF. As we hypothesized in the chloride and bromide complexes, the presence of an equilibrium in the solvent adducts cannot be ruled out. On the basis of the data provided here, we cannot definitively state the species involved in this equilibrium.

The electrochemical properties of the iron(II) precursors have been examined in DMF (Figures 5 and S7 in the Supporting Information and Table 3). Each of the halide complexes exhibits a quasi-reversible one-electron oxidative wave. The oxidation potentials of the various complexes shift depending upon the identity of the ancillary ligands. Examination of the chloride and bromide complexes shows a positive potential shift of 118 mV for the bromide species (i.e., the chloride is more easily oxidized). Upon a change of the fifth ligand from a halide to a solvent molecule(s), a further positive shift is observed. The average of the potentials for the $Fe^{2+/3+}$ couple for the complexes **3**, **4**, and *trans*-$[Fe(qn)_2(PrOH)_2]$ is −166 mV (vs $Fc^{+/0}$), a 168 mV shift in the positive direction from the chloride complex **1**. The voltammograms of **3**, **4**, and *trans*-$[Fe(qn)_2(PrOH)_2]$ in DMF all exhibit behavior consistent with a chemical step after an initial oxidation (Figure S8 in the Supporting Information). This reduction peak does not grow larger with repeated electrochemical cycles.

Substitution of the quinoline ring also affects the potential of the $Fe^{2+/3+}$ couple as it appears at −393 mV (vs $Fc^{+/0}$) for **4-MeO-1**, making it more easily oxidized by 59 mV. The introduction of the methoxy group at the 4 position of the quinoline ring introduces ligand noninnocence within the potential range studied (Figure S7 in the Supporting Information). The other iron(II) quinaldate complexes do not exhibit this behavior. Of the many $Fe^{II/III}$ couples known,[33,34] these quinaldate species are most similar to FeSOD[35] and iron complexes of tetraazamacrocycles.[36]

Summary and Implications

The synthesis and physical properties of a series of iron(II) quinaldates are described. The structures of three coordinatively unsaturated iron(II) quinaldates are reported. Yet, the ^{1}H NMR spectra of these complexes in DMF (i.e., a coordinating solvent) provide evidence for the formation of six-coordinate DMF adducts in the anionic complexes. Therefore, the results strongly suggest that the solid-state structures do not reflect the composition of these samples in solution. At this stage, both geometric isomers (cis and trans) are possible, but the ligands must be in symmetric environments. On basis of a comparison with **4-MeO-1**, the major species in **1** is the six-coordinate DMF adduct. In the solvent adducts, the major species may be either five-coordinate or six-coordinate.

The electronics of the metal center can be tuned via substitution of the aromatic quinaldate ring or the ancillary ligands. The electrochemical potentials and electronic spectra point to cursory descriptions of the electronic structure. Assuming that the energy levels of the π^* orbitals of the quinaldate ligands are stationary, the electronic transition of the metal-to-ligand charge-transfer bands are indicative of the energy levels of the metal orbitals. The charge-transfer transition for the chloride occurs at lower energy than that of the bromide. Therefore, a lower oxidation potential of the chloride species is expected, and one is indeed observed. Introduction of the 4-methoxy group in the quinaldate ring shifts the charge-transfer bands to higher energy than those in the unsubstituted complex **1**. This indicates a widening in the gap between the metal orbitals and the ligand π^* orbitals, due to either a lowering of the energy of the metal orbitals or an increase in energy of the π^* orbitals (or a combination of the two). The more negative shift for the $Fe^{2+/3+}$ couple for the **4-MeO-1** complex relative to **1** indicates that the methoxy group causes a destabilization (increase in energy) of the metal orbitals, consistent with a stronger donor. Similar effects have been observed in other pyridine-rich ligands.[31] The DMF adduct has a potential that is less positive than the halides, consistent with its electronic spectrum and its increased air stability.

Quinaldic acid has been utilized as an additive in both Fenton and Gif hydrocarbon oxidation systems.[37−40] While the typical solvent for Fenton chemistry is water, pyridine is characteristically used in Gif systems. Elemental iron reacts

(33) Groni, S.; Hureau, C.; Guillot, R.; Blondin, G.; Blain, G.; Anxolabéhère-Mallart, E. *Inorg. Chem.* **2008**, *47*, 11783−11797.
(34) Mehn, M. P.; Fujisawa, K.; Hegg, E. L.; Que, L., Jr. *J. Am. Chem. Soc.* **2003**, *125*, 7828–7842.
(35) Vance, C. K.; Miller, A.-F. *Biochemistry* **2001**, *40*, 13079–13087.
(36) Hubin, T. J.; McCormick, J. M.; Collinson, S. R.; Buchalova, M.; Perkins, C. M.; Alcock, N. W.; Kahol, P. K.; Raghunathan, A.; Busch, D. H. *J. Am. Chem. Soc.* **2000**, *122*, 2512–2522.
(37) Shul'pin, G. B. *J. Mol. Catal. A: Chem.* **2002**, *189*, 39–66.
(38) Barton, D. H. R.; Hu, B.; Rojas Wahl, R. U.; Taylor, D. K. *New J. Chem.* **1996**, *20*, 121–124.
(39) Bianchi, D.; Bortolo, R.; Tassinari, R.; Ricci, M.; Vignola, R. *Angew. Chem., Int. Ed.* **2000**, *39*, 4321–4323.
(40) Kiani, S.; Tapper, A.; Staples, R. J.; Stavropoulos, P. *J. Am. Chem. Soc.* **2000**, *122*, 7503–7517.

with quinaldic acid in pyridine to yield *trans*-$[Fe(qn)_2(pyr)_2]$.[18] Although iron(II) salts are typically employed as the starting materials in these oxidations, the identity of the species responsible for hydrocarbon oxidation remains elusive. Furthermore, the identity of the active oxidant and the product distributions can be significantly altered by the presence of either a weakly or strongly coordinating ligand.[41] This was one of the reasons why we are interested in the constitution of iron(II) quinaldates.

In a recent report, a quinaldate-supported bis(μ-hydroxy)-diiron(III) species reacts with hydrogen peroxide in the presence of a base to yield a mononuclear iron(III) peroxo.[42] Reaction with carbon dioxide then yields an iron(III) peroxycarbonate adduct, which, upon warming, reversibly cleaves the O−O bond.[42,43] Few examples of first-row transition-metal complexes that catalyze O−O bond formation and cleavage are known.[44−47] While second- and third-row transition-metal peroxycarbonates have been known for some time,[48−52] first-row transition-metal peroxycarbonates are far more rare.[53−55] Suzuki's peroxycarbonate is the only first-row peroxycarbonate adduct that has been structurally characterized. Although peroxycarbonate itself is a potent oxidant for organic substrates,[56−58] metal peroxycarbonate species have been postulated in a number of catalytic schemes,[59] green oxidations,[60] and biological processes.[61−64] Early proposals invoked various roles for bicarbonate at the oxygen-evolving cluster of photosystem II;[65,66] however, later studies discount the role of bicarbonate in water oxidation.[67] Our laboratory is exploring alternate routes for first-row transition-metal peroxycarbonate generation.

Acknowledgment. M.P.M. thanks the University of Wyoming for start-up funds to support this work. Financial support by the NSF (Grant CHE 0619920) for the purchase of the Bruker Apex II diffractometer is gratefully acknowledged. D.T.H. was supported by an NSF-GK-12 (Grant DGE-0538642) fellowship and a graduate fellowship from NCRR and Wyoming INBRE (Grant P20RR016474) during separate portions of this work. We gratefully thank Teresa Lehmann for assistance with the set-up of the T_1 measurements.

Supporting Information Available: Table S1 with detailed metrics for all known iron(II) quinaldates; Figure S1 with IR data; Figure S2 with an electronic spectrum of **4-MeO-1**; Figures S3−S6 with variable-temperature ^{1}H NMR data, Figure S7 with CV data for substituted quinaldate complexes, Figure S8 with CV data for **4**, and crystallographic data in CIF format. This material is available free of charge via the Internet at http://pubs.acs.org.

(41) Mekmobche, Y.; Ménage, S.; Toia-Duboc, C.; Fontecave, M.; Galey, J.-B.; Lebrun, C.; Pécaut, J. *Angew. Chem., Int. Ed.* **2001**, *40*, 949–952.
(42) Hashimoto, K.; Nagatomo, S.; Fujinami, S.; Furutachi, H.; Ogo, S.; Suzuki, M.; Uehara, A.; Maeda, Y.; Watanabe, Y.; Kitagawa, T. *Angew. Chem., Int. Ed.* **2002**, *41*, 1202–1205.
(43) Furutachi, H.; Hashimoto, K.; Nagatomo, S.; Endo, T.; Fujinami, S.; Watanabe, Y.; Kitagawa, T.; Suzuki, M. *J. Am. Chem. Soc.* **2005**, *127*, 4550–4551.
(44) Halfen, J. A.; Mahapatra, S.; Wilkinson, E. C.; Kaderli, S.; Young, V. G., Jr.; Que, L., Jr.; Zuberbühler, A. D.; Tolman, W. B. *Science* **1996**, *271*, 1397–1400.
(45) Limburg, J.; Brudvig, G. W.; Crabtree, R. H. *J. Am. Chem. Soc.* **1997**, *119*, 2761–2762.
(46) Mirica, L. M.; Ottenwaelder, X.; Stack, T. D. P. *Chem. Rev.* **2004**, *104*, 1013–1045.
(47) Hatcher, L. Q.; Karlin, K. D. *J. Biol. Inorg. Chem.* **2004**, *9*, 669–683.
(48) Hayward, P. J.; Blake, D. M.; Nyman, C. J.; Wilkinson, G. *Chem. Commun.* **1969**, 987–988.
(49) Hayward, P. J.; Blake, D. M.; Wilkinson, G.; Nyman, C. J. *J. Am. Chem. Soc.* **1970**, *92*, 5873–5878.
(50) Clark, H. C.; Goel, A. B.; Wong, C. S. *J. Organomet. Chem.* **1978**, *152*, C45–C47.
(51) Aresta, M.; Tommasi, I.; Quaranta, E.; Fragale, C.; Mascetti, J.; Tranquille, M.; Galan, F.; Fouassier, M. *Inorg. Chem.* **1996**, *35*, 4254–4260.
(52) Aresta, M.; Fragale, C.; Quaranta, E.; Tommasi, I. *J. Chem. Soc., Chem. Commun.* **1992**, 315–317.
(53) Aresta, M.; Nobile, C. F. *J. Chem. Soc., Dalton Trans.* **1977**, 708–711.
(54) Schappacher, M.; Weiss, R. *Inorg. Chem.* **1987**, *26*, 1189.
(55) Schappacher, M.; Weiss, R.; Montiel-Montoya, R.; Trautwein, A.; Tabard, A. *J. Am. Chem. Soc.* **1985**, *107*, 3736–3738.
(56) Bennett, D. A.; Yao, H.; Richardson, D. E. *Inorg. Chem.* **2001**, *40*, 2996–3001.
(57) Richardson, D. E.; Yao, H.; Frank, K. M.; Bennett, D. A. *J. Am. Chem. Soc.* **2000**, *122*, 1729–1739.
(58) Yao, H.; Richardson, D. E. *J. Am. Chem. Soc.* **2003**, *125*, 6211–6221.
(59) Lane, B. S.; Vogt, M.; DeRose, V. J.; Burgess, K. *J. Am. Chem. Soc.* **2002**, *124*, 11946–11954.
(60) Ember, E.; Rothbart, S.; Puchta, R.; van Eldik, R. *New J. Chem.* **2009**, *33*, 34–49.
(61) Borowski, T.; Bassan, A.; Richards, N. G. J.; Siegbahn, P. E. M. *J. Chem. Theory Comput.* **2005**, *1*, 686–693.
(62) Chang, C. H.; Richards, N. G. J. *J. Chem. Theory Comput.* **2005**, *1*, 994–1007.
(63) Elam, J. S.; Malek, K.; Rodriguez, J. A.; Doucette, P. A.; Taylor, A. B.; Hayward, L. J.; Cabelli, D. E.; Valentine, J. S.; Hart, P. J. *J. Biol. Chem.* **2003**, *278*, 21032–21039.
(64) Liochev, S. I.; Fridovich, I. *Proc. Natl. Acad. Sci. U.S.A.* **2004**, *101*, 12485–12490.
(65) Baranov, S. V.; Ananyev, G. M.; Klimov, V. V.; Dismukes, G. C. *Biochemistry* **2000**, *39*, 6060–6065.
(66) Baranov, S. V.; Tyryshkin, A. M.; Katz, D.; Dismukes, G. C.; Ananyev, G. M.; Klimov, V. V. *Biochemistry* **2004**, *43*, 2070–2079.
(67) Ulas, G.; Olack, G.; Brudvig, G. W. *Biochemistry* **2008**, *47*, 3073–30075.